



A reconstruction of the East Asian summer monsoon index over the half past millennium

Feng Shi*, Hugues Goosse, Jianping Li, Fredrik Charpentier Ljungqvist, Sen Zhao, Ting Liu, Qiuzhen Yin, Zhengtang Guo

2020.05.05

Outline

- Introduction
- Data and Method
- Results
- Mechanism
- Conclusions

Introduction

- **Obverse:** More precipitation = strong monsoon
 - Proxy data (paleoclimate) (e.g. Liu et al., 2019)
- **Reverse:** More meiyu precipitation = weak monsoon
 - Instrumental record (e.g. Wang et al., 2008)

Comparison of the EASMI and MJJAS precipitation in China

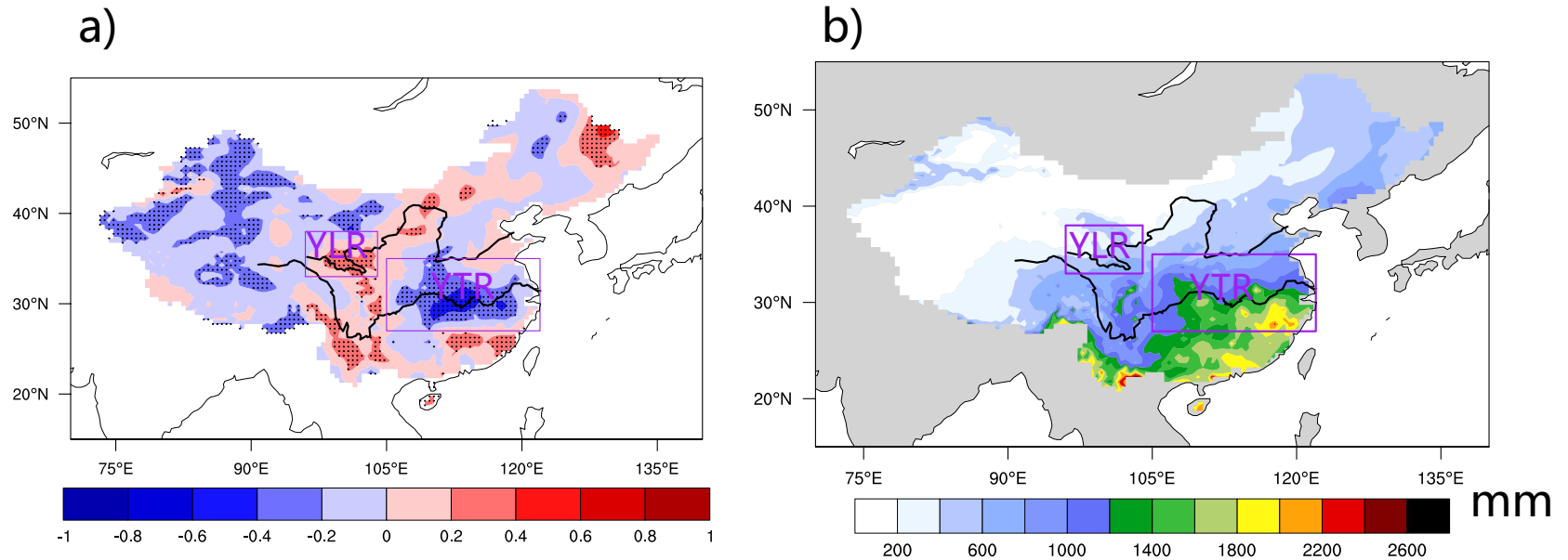


Figure 1. The information of the study area. a) the relationship between the East Asian summer monsoon index with warm season (May to September) precipitation in China during the period AD 1961-2018, b) the average annual precipitation during the same period. Two boxes indicate two sub regions (Yangtze River valley (27°N–35°N, 105°E–122°E) and Yellow River valley (33°N–38°N, 96°E–104°E))

Outline

- Introduction
- Data and Method
- Results
- Mechanism
- Conclusions

Data

- $0.5^\circ \times 0.5^\circ$ instrumental monthly precipitation in AD 1961-2018
 - 2472 meteorological stations (Zhao et al., 2015)
- $0.5^\circ \times 0.5^\circ$ reconstructed MJJAS precipitation in AD 1470-2000
 - 371 tree-rings and 107 DF indices (Shi et al., 2017)
- Assimilated CESM-LME in AD 850-2005
 - 12 members (96 latitudes \times 144 longitudes) (Otto-Bliesner, et al., 2016)
 - Particle filter based on the reconstructed MJJAS precipitation

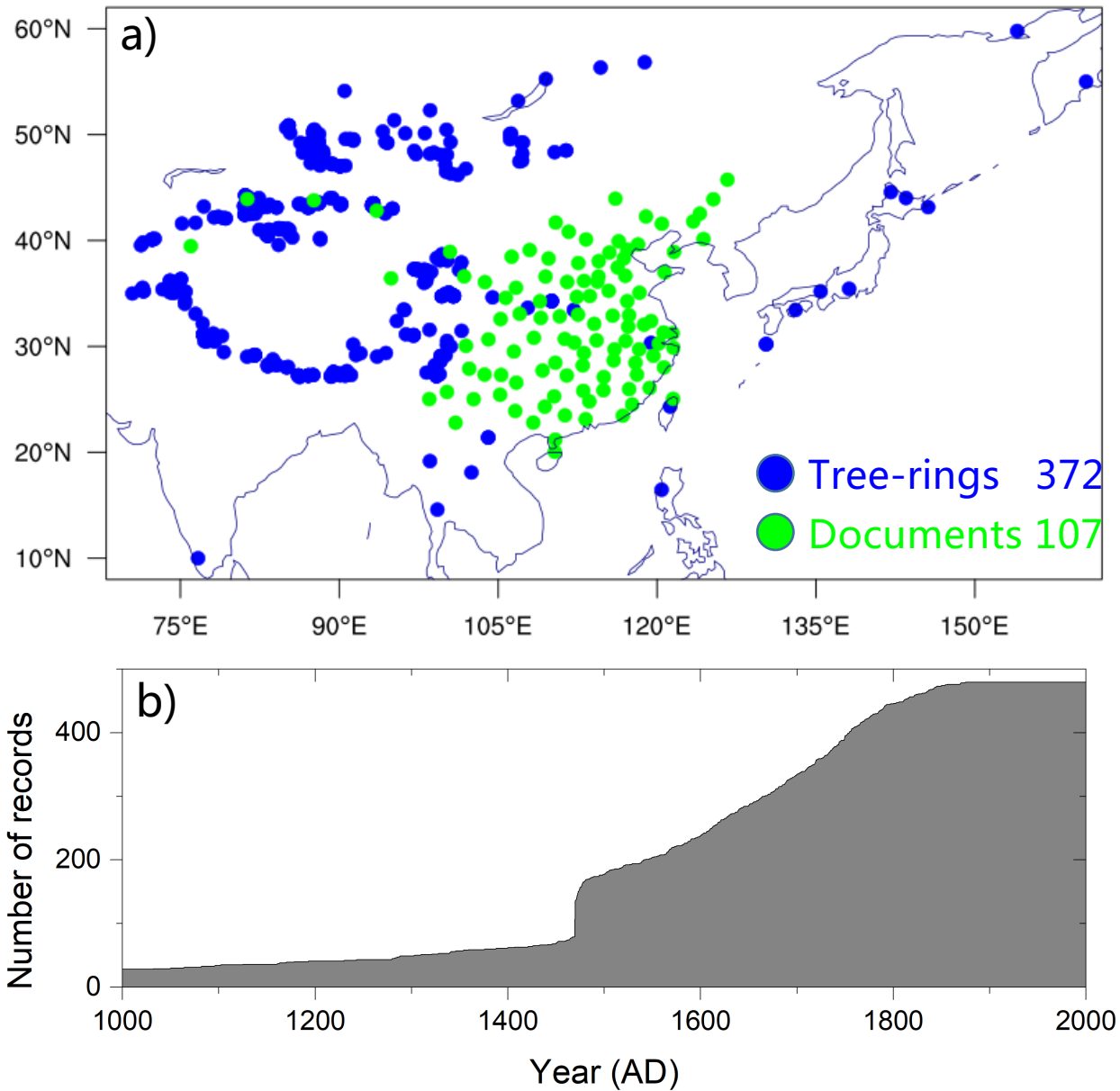


Figure 2. Map showing the locations of proxy records (a) and plot of the first year covered by each proxy record (b) (Shi et al., 2017)

Method: Optimal information extraction (OIE)

“The OIE method was derived from the CPS method, and developed with several versions inspired by the local (LOC) method, a Bayesian framework (BARCAST), the generalized likelihood uncertainty estimation method, and the ensemble reconstructions” (PAGES 2k Consortium, 2019)

Procedures:

- 1) The correlation coefficient between the target and local instrumental climate as weight is used
- 2) The regression coefficients are random variables within the ranges of the linear and inverse regressions
- 3) The generalized likelihood uncertainty estimation method is used to estimate the uncertainty

Advantages:

- 1) Measure regional differences in the response of each record to the climate
- 2) Efficiently retain low-frequency climate signals

Drawback:

An overfitting tendency: An independent test data is needed

(Shi et al., 2014; 2015; 2017)

Outline

- Introduction
- Data and Method
- Results
- Mechanism
- Conclusions

Comparison of the reconstructed and instrumental EASM indices

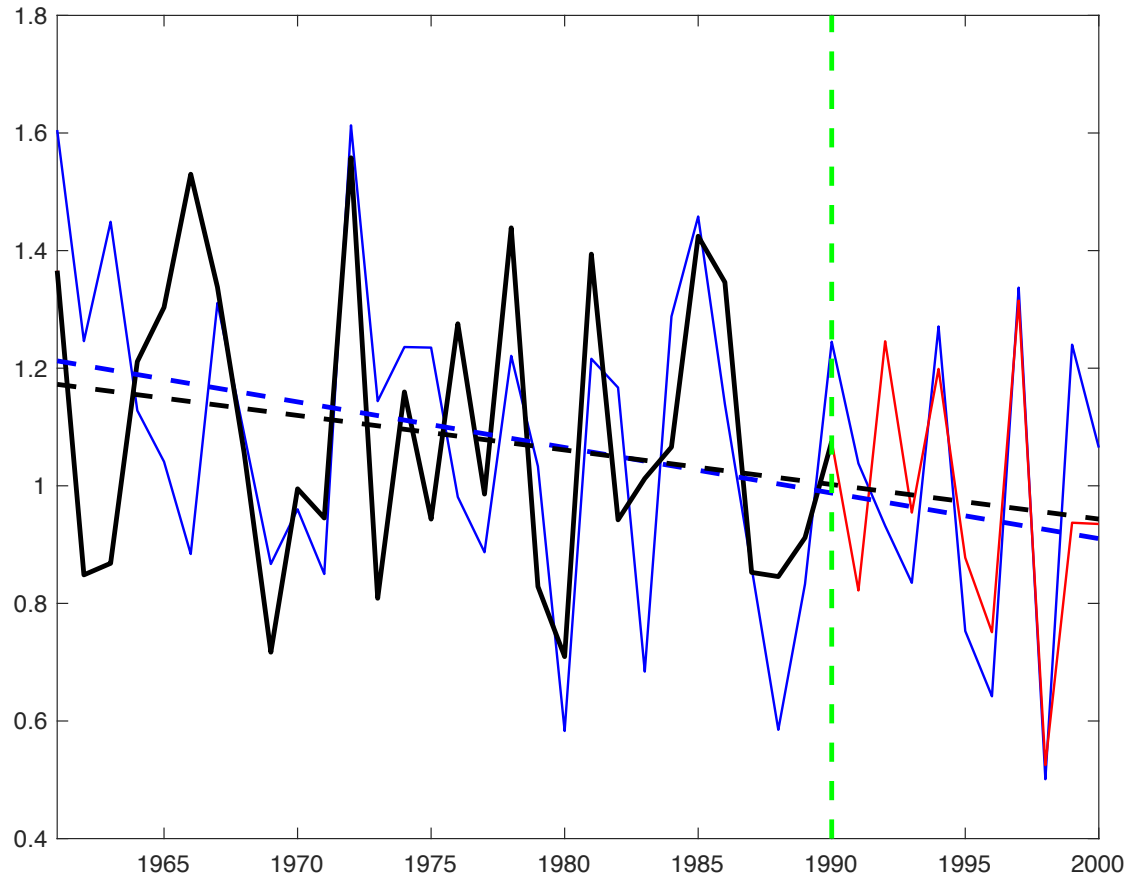


Figure 3. Comparison of the reconstructed and instrumental EASM indices. The blue line is the instrumental index from the instrumental wind field. The black line is the reconstructed index from the proxy-based precipitation. The dashed lines are their long-term linear trends. The vertical green line is the dividing line between the calibration period (AD 1961–1990) and the verification period (AD 1991–2000)

Spectral analysis of the reconstructed EASMI

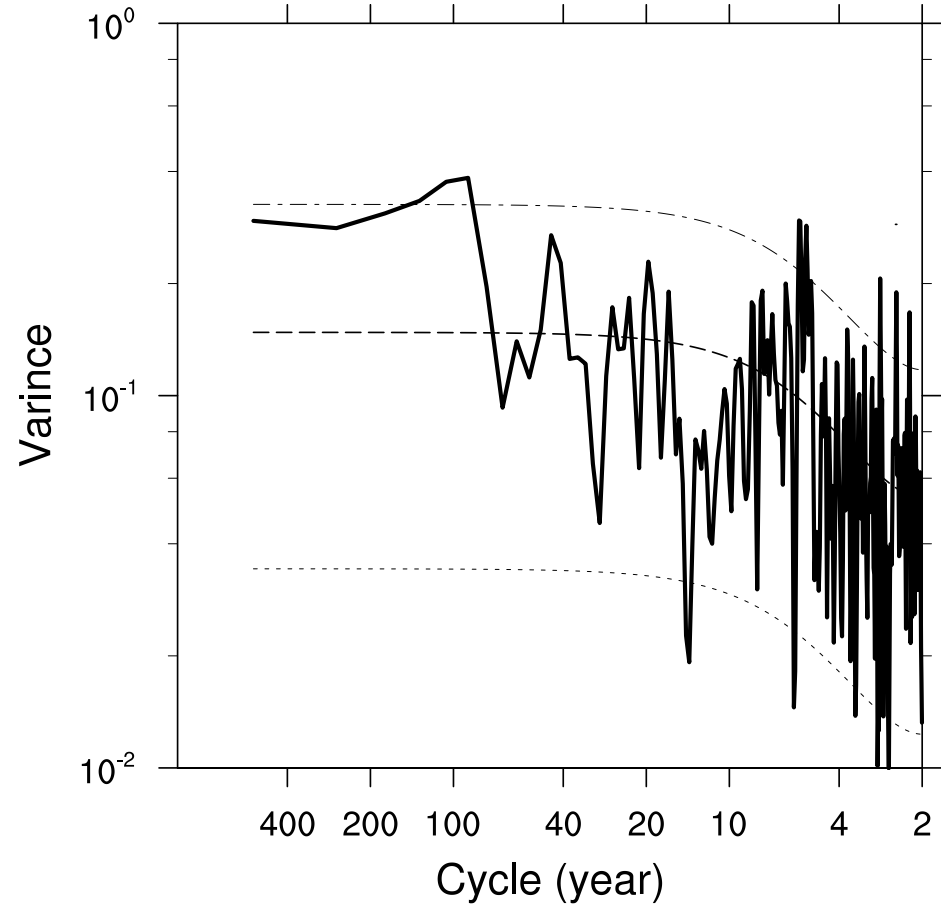


Figure 4. Spectral analysis of the reconstructed EASMI

EEMD analysis of the reconstructed EASMI

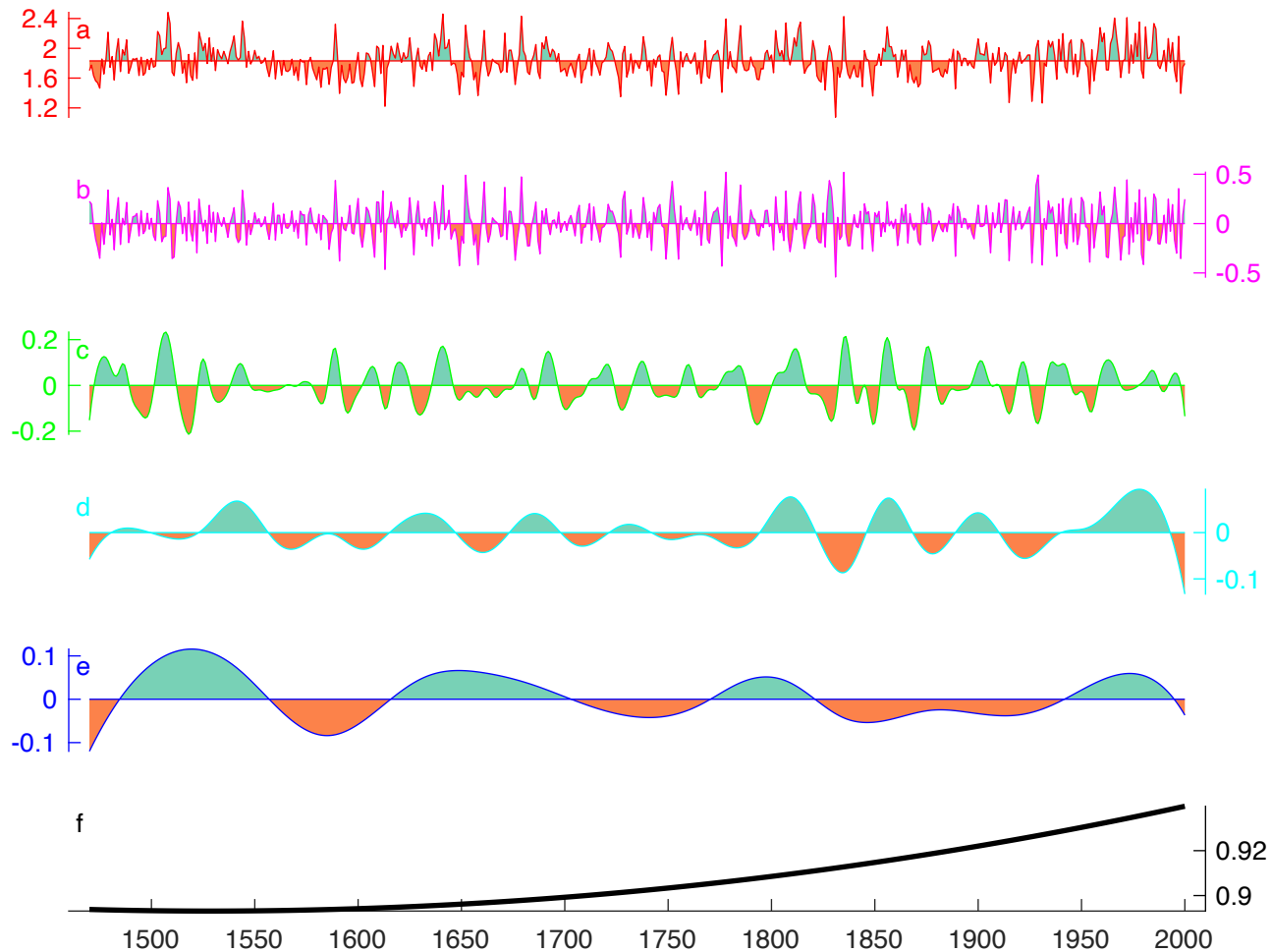


Figure 5. EEMD analysis of the reconstructed EASMI index. (a) the raw reconstruction, (b) inter-annual component, (c) inter-decadal component, (d) multi-decadal component, (e) centennial component, (f) non-linear trend.

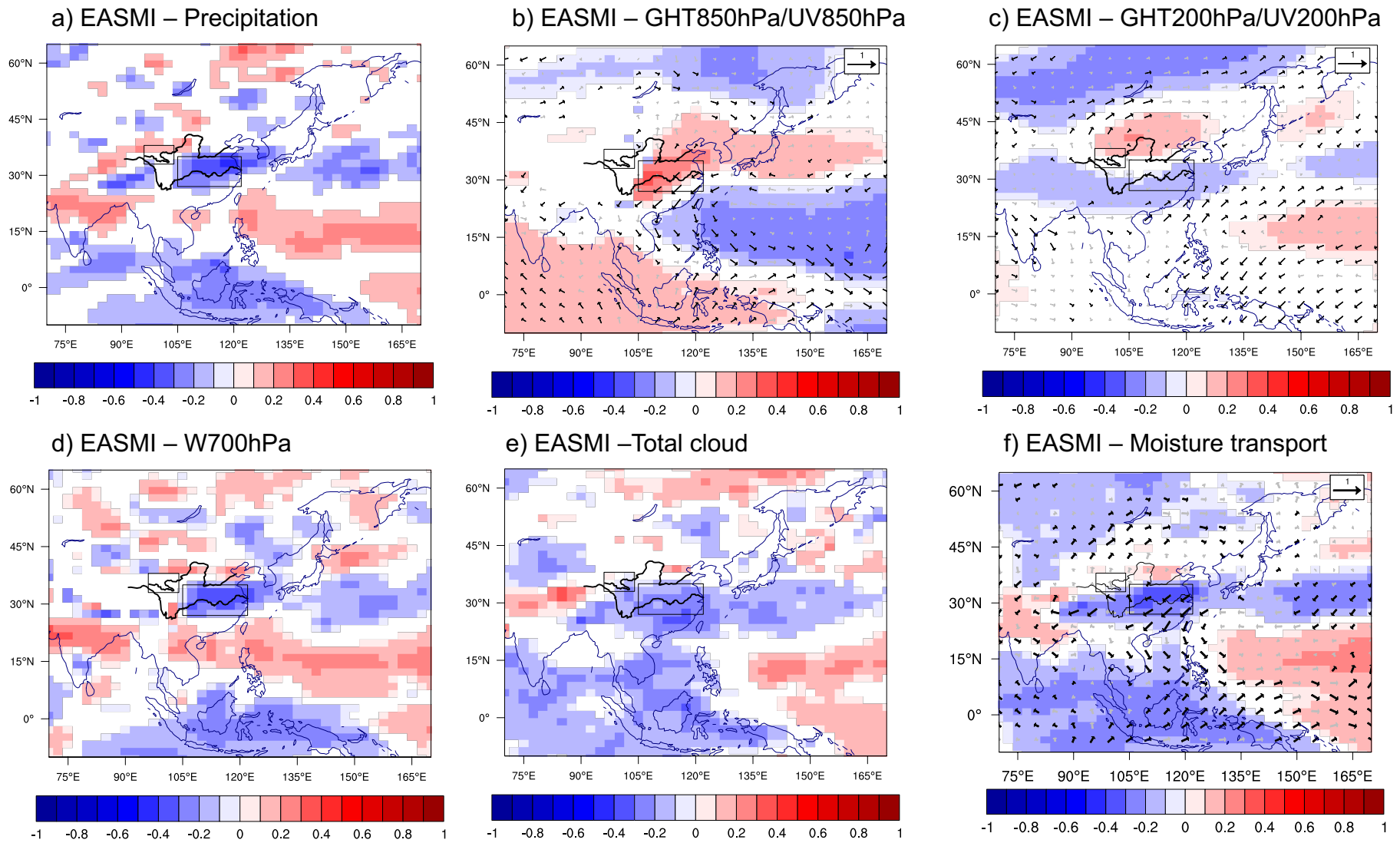


Figure 6. Correlation of the proxy-based EASMI index over the whole period 1470–2000 CE with data assimilation-based summer (JJA) anomaly patterns for (a) precipitation (shading), (b) the 850-hPa wind field (vector) and 850-hPa geopotential height (shading), (c) 200-hPa wind (vector) and 200-hPa geopotential height (shading), (d) 700-hPa vertical velocity ($-\omega$, shading), (e) total cloud fraction (shading), and (f) vertical integral moisture transport (vector) and precipitable water (shading). The white area indicate that the correlation does not exceed the 90% significant level based on a student's t-test. The black arrow is the correlation at the 90% significant level. Gray arrows indicate a student's t-test failure.

Outline

- Introduction
- Data and Method
- Results
- Mechanism
- Conclusions

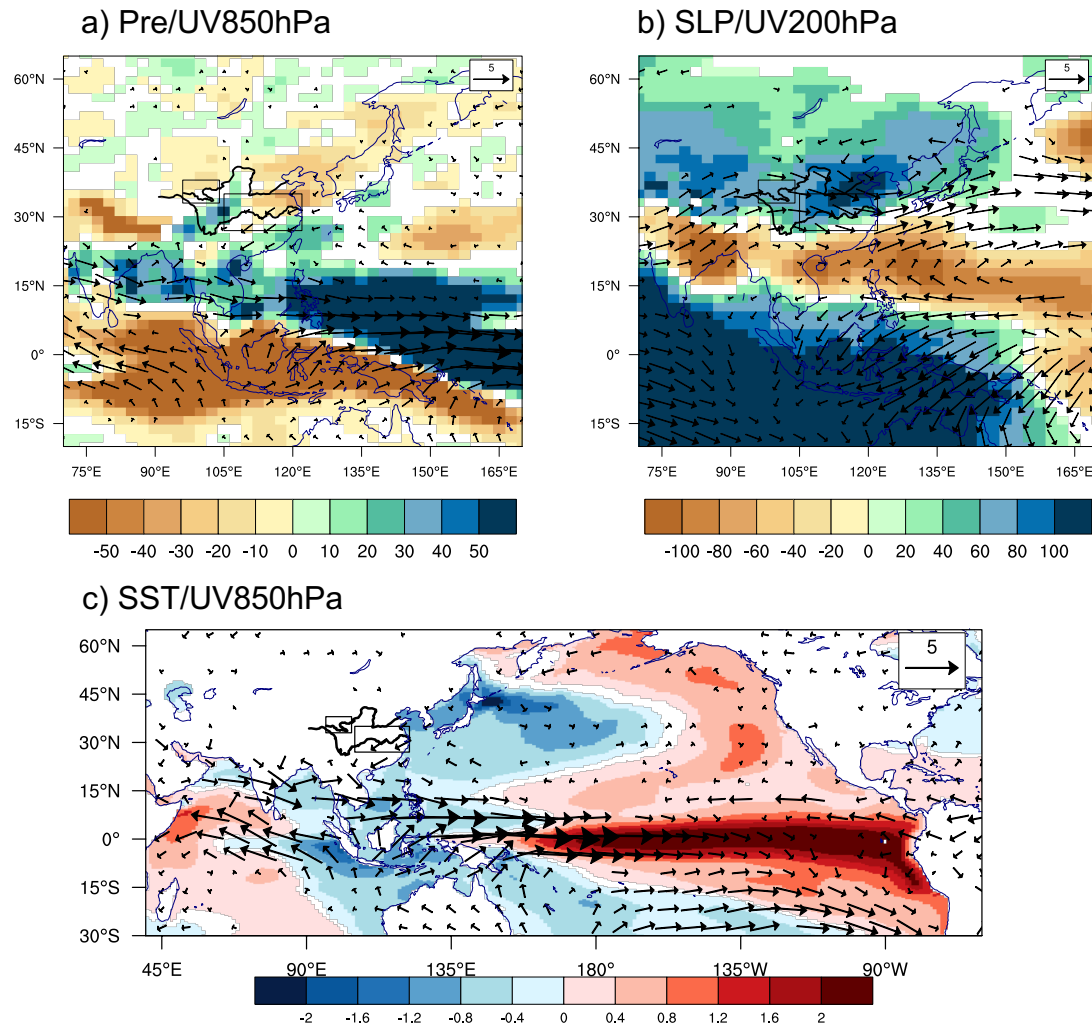


Figure 7. Differences of El Niño (81 events) minus La Niña (65 events) for summer (JJA) mean precipitation and 850-hPa wind (a), sea level pressure and 200-hPa wind (b), and differences between strong EASM (77) and weak EASM (83) events)for surface sea temperature and 850-hPa wind (c). The white areas denote the 90% statistical significance level using the Student's t-test.

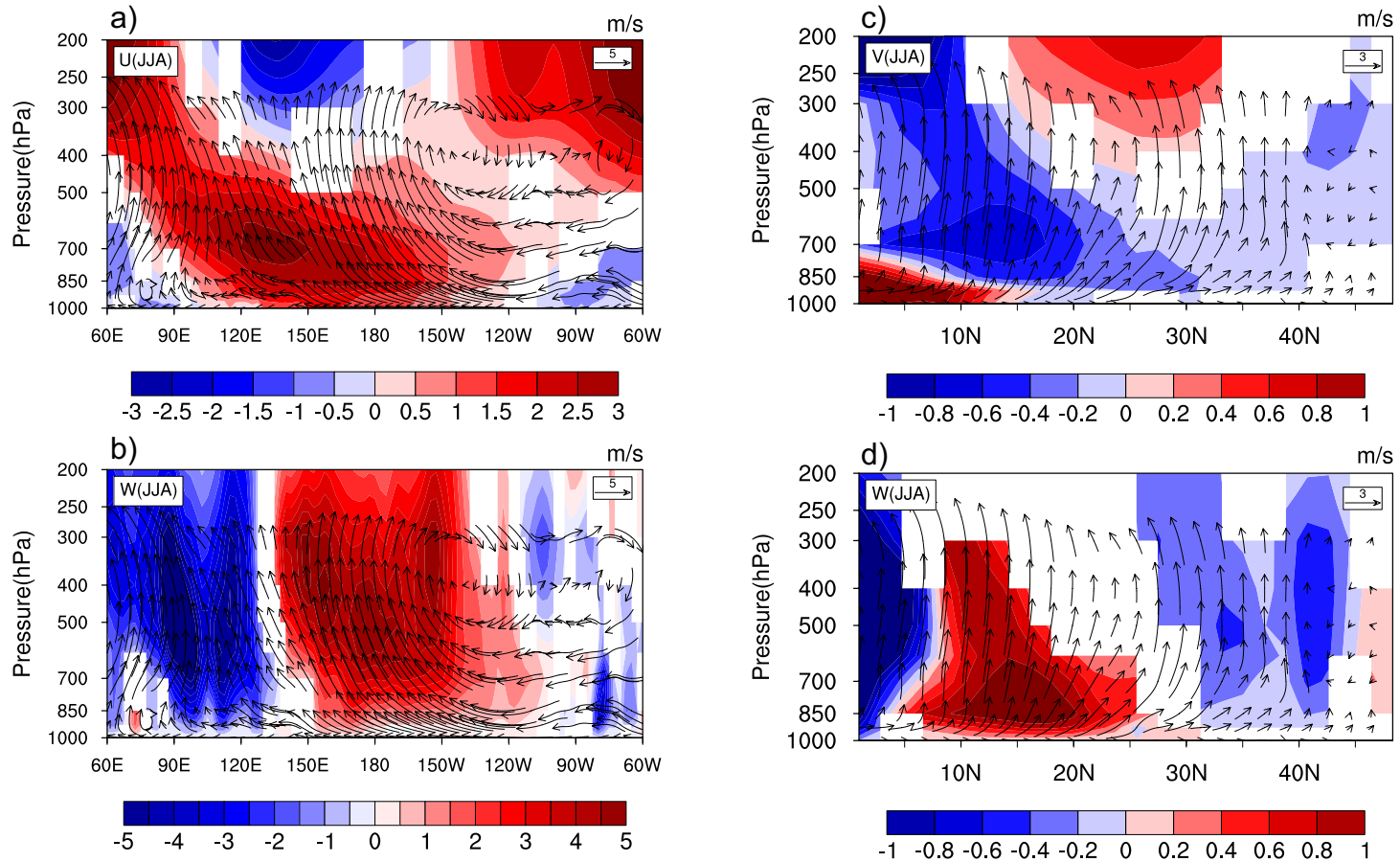


Figure 8. Differences of El Niño (81 events) minus La Niña (65 events) for summer (JJA) vertical velocity ($-\Omega$) (a) and meridional velocity (b) over East Asia (along 20° S– 20° N mean), summer (JJA) vertical velocity ($-\Omega$) (c) and zonal velocity (d) over East Asia (along 70° – 140° E mean). Shading indicates the anomalies, and the climatology is indicated by vectors. The white areas indicate that the difference does not exceed the 90% confidence level based on a Student's t-test.

Conclusions

- The EASM index covering 1470–2000 CE is reconstructed
- Our EASM index reconstruction complements and improve the interannual to decadal scale information compared to previous low-resolution monsoon reconstructions
- This index could be used to represent the seesaw pattern for the drought/flood variability in monsoon core and fringe regions
- The dominate inter-annual EASM variability is linked to ‘ENSO-like’ sea surface temperature anomalies

Thank you for your attention!